



Influence of Preheating on Lamellar Gray Cast Iron for Surface Layer Welding applications with Plasma-Transferred Arc Powder and Metal Inert Gas Welding Processes with Duplex Steel as Filler Material

U. Reisgen¹ · M. Oechsner² · R. Sharma¹ · J. Ellermeier³ · G. Andersohn⁴ · T. Engler⁵ · E. Zokoll¹ · B. Heider⁵ · E. Gonzalez Olivares¹

Submitted: 11 November 2019 / in revised form: 21 February 2020 / Published online: 18 March 2020
© The Author(s) 2020

Abstract The good capacity of gray cast iron for the manufacture of complex geometry components is widely recognized, but its low resistance to corrosion and low weldability complicate the use of this material for some industrial applications. The corrosion resistance can be improved by metallic surface layers using welding processes with low percentages of dilution between the filler and base material. However, the welding processes impose very high heat load on the base material, which in the case of cast iron could promote the formation of hard and brittle microstructures, facilitating the formation of cracks. This work deals with weld beads of duplex steel on lamellar gray cast iron made either by plasma-transferred arc powder (PTA-P) or by metal inert gas (MIG) using the cold metal transfer (CMT) technology, with emphasis on achieving low dilution, hardness and imperfections (internal porosities). Preheating was used to reduce the hardness in the heat-affected zone, while different levels of helium were added in the shielding gas to study its effect on the

geometry and hardness of the weld beads. The results showed that the PTA-P process resulted in lower values of dilution and hardness because of a low cooling rate compared to that of the MIG-CMT process. In addition, it was observed that preheating the base material reduced the hardness of the heat-affected zone but increased the dilution of the weld bead.

Keywords Cast iron · Cladding · CMT · Duplex steel · PTAW < processing · Preheating of substrate < processing

Introduction

For geometrically complex, flow-optimized components like pump casings, casting is the production method of choice. To produce as economical as possible, gray cast iron with lamellar graphite can be used. Yet corrosion, cavitation and abrasive materials can make higher alloyed base materials necessary, resulting not only in reduced castability, but also in higher production costs because expensive alloys are also present in areas without exposition to the medium (Ref 1-3). Through the surface layer located in the areas affected by corrosion, cavitation and abrasion, it is possible to reduce costs, increasing the effectiveness and life of the component (4-11).

A cast iron alloy is defined as an iron-carbon-based alloy containing more than 2.06 wt.% carbon. The carbon is deposited in the mostly ferritic-pearlitic structure as graphite. By adding alloying elements like manganese, it is possible to modify the geometrical form of those depositions resulting in different mechanical-technological properties. While heat treatments can change the metal matrix as well as the properties of the cast iron, the

✉ E. Gonzalez Olivares
gonzalez@isf.rwth-aachen.de

¹ Rheinisch Westfälische Technische Hochschule Aachen
Institut für Schweistechnik und Fügetechnik, Arc Welding,
Aachen, Germany

² Technische Universität Darmstadt Zentrum für
Konstruktionswerkstoffe, Darmstadt, Germany

³ Technische Universität Darmstadt Zentrum für
Konstruktionswerkstoffe, Mess- und Kalibriertechnik,
Darmstadt, Germany

⁴ Aalberts Surface Treatment GmbH, Kerpen, Germany

⁵ Technische Universität Darmstadt Zentrum für
Konstruktionswerkstoffe, Oberflächentechnik, Darmstadt,
Germany

geometrical forms of the graphite do not change. An important challenge in the surface layer of cast iron materials is graphite, which can appear in vermicular, spherical or lamellar form, which is a source of carbon that diffuses to other regions of the material, which facilitates the formation of martensite and ledeburite structures (Ref 12). For this reason, the weldability of cast irons depends on their original matrix structure, chemical composition, mechanical properties, welding process and working conditions (Ref 13). When the cast iron is welded, three zones can be identified in metallographic cross sections of the weld beads, the fusion zone (FZ), where the base metal is mixed with the filler material, characterized by high cooling rates producing very hard and brittle microstructures. The partially melted zone (PMZ) borders the FZ and is formed by the portion of the matrix of the base metal near the primary graphites melted during the welding pass. In the heat-affected zone (HAZ), the peak temperature rises above the critical point. There is no fusion, but the matrix is transformed into austenite during heating. During cooling, a variety of microstructure transformations is obtained (Ref 13–15).

The formation of carbides, ledeburite and martensite structures in different zones of the weld bead promotes the formation of cracks in the base material, due to the high hardness that is achieved (Ref 15). As a general procedure to prevent the formation of these cracks, thermal treatments before and after welding are recommended (Ref 13–16). Preheating temperatures are generally in the range of 300–600 °C. According to (Ref 17), a preheat temperature of 540 °C is necessary for a significant reduction in hardness in the FZ and the HAZ when gray cast iron is welded with mild steel electrodes. However, to improve the machinability of welded cast iron a post-weld heat treatment (PWHT) is also necessary. Very slow cooling curves can prevent the formation of eutectic carbides during solidification in the PMZ, while typical preheating temperatures often tend to increase the quantity and continuity of the carbides instead of reducing their formation (Ref 14).

To avoid hardening and crack formation in the HAZ, the cooling times need to be long, which can be achieved by preheating and high heat input per unit length (Fig. 1) (Ref 12, 16, 18). Yet, this is a contradiction to the demand for low dilution.

Welding Processes

For surface layer welding on cast iron, there are many processes already known as suitable, for example gas powder welding, plasma-transferred arc (PTA) welding, metal inert gas (MIG) welding as well as manual metal arc (MMA) welding with a stick electrode (Ref 12, 16, 18–20).

Usually dilutions up to 10–15% are suggested for good surface weldings to maintain the aimed properties of the weld surface material (Ref 21). Aside the PTA process, the MIG welding process in its variant called cold metal transfer (CMT) seems suitable due to its low heat input and material transfer in the short phase to create those surface layers. In preceding works (Ref 22, 23), it has been found that the MIG-CMT process is suitable to make welds on the gray cast iron, with low dilutions and increasing its resistance to corrosion by means of coatings with duplex stainless steel.

The CMT process is a modified variant of the short-circuit metal transfer mode characterized by low energy levels, achieved by a combination of electronical regulation and enforced retraction of the welding wire in order to improve the droplet detachment. This improved variant of the classical short arc process has been known for years (Ref 24). During the arc phase, the current and voltage and therefore the arc length and heat input can be adjusted to ensure the molten pool formation and the melting of the filler material. The following short-circuit phase uses a combination of electronic current control and mechanical retraction of the wire to assure a spatter-reduced transfer of the molten filler wire as well as a reduced current for re-ignition of the arc. With the MIG-CMT process, surface layers on nickel alloys with dilutions of 3% have been achieved showing its suitability for low heat input clad welding using a wire to produce the weld clad (Ref 25).

On the other hand, the plasma-transferred arc powder (PTA-P) welding process is characterized by a pilot arc established between the tungsten electrode and the constrictor nozzle. This pilot arc has a current between 5 and 50 A, and its objective is to provide ionized plasma for ignition of the main arc (Fig. 2). The main arc is characterized by its columnar shape and its high energy levels. The filler material in powder form is added by holes near the main arc hole in the constricting nozzle. The powder particle morphology influences the process. Spherical particles are preferred over particles of irregular shape as they exhibit poor feeding characteristics (Ref 26). However, the production costs of spherical particles are high, as they are made by an atomization process which involves nitrogen or argon (Ref 27, 28). The number of holes and the arrangement of them in the constricting nozzle vary depending on the manufacturer of the product (Fig. 2). This welding process is characterized by obtaining low levels of dilution, between 3 and 8% for the Stellite 6 alloy as an example (Ref 29). The PTA-P process is considered to be difficult to set up welding process, due to the numerous parameters that must be considered for producing a weld. The main parameters are: electrode diameter, constriction nozzle diameter, flow rate of the plasma gas, shielding gas and transport gas and the powder feed rate.

Fig. 1 Crack formation in HAZ while cladding cast iron

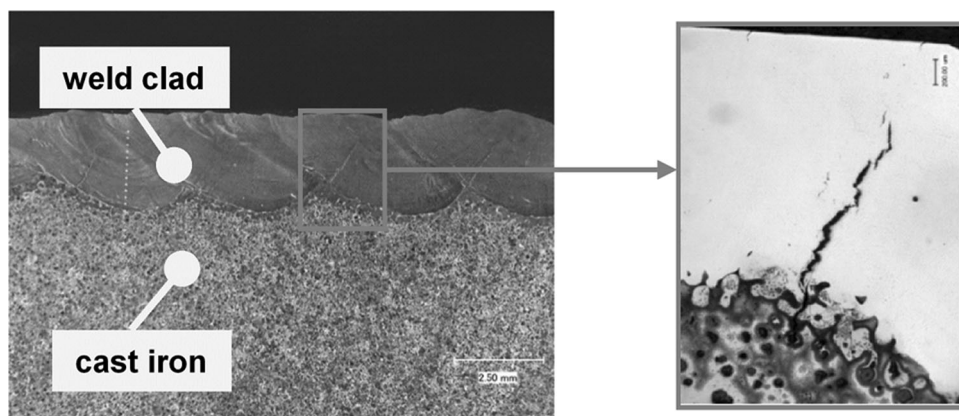
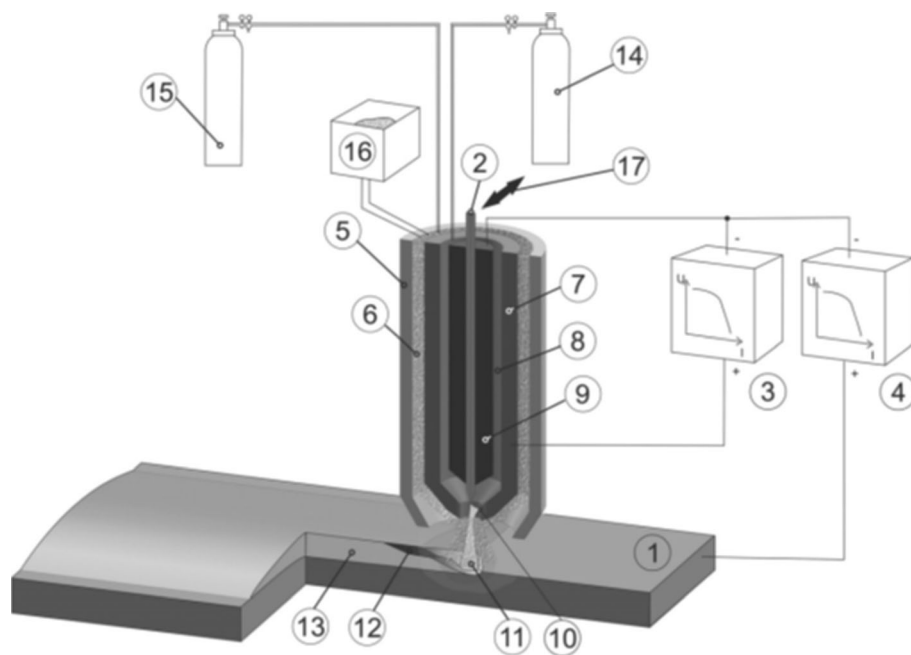


Fig. 2 Schematic of the plasma-transferred arc (PTA) welding process with powder as addition material: (1) base material, (2) tungsten electrode, (3) pilot arc electrical circuit, (4) main arc electrical circuit, (5) shielding gas nozzle, (6) feeding gas and powder, (7) constriction nozzle, (8) plasma gas, (9) cathode clamping device, (10) pilot arc, (11) main arc, (12) molten pool, (13) surface layer, (14) plasma gas supply, (15) shielding and feeding gas supply, (16) powder supply, (17) oscillation (Ref 30, 31)



The shielding gas in the welding processes, besides having the important mission of isolating the molten pool from the atmosphere, also has additional effects (no less important than the main function), such as stabilizing the arc, controlling the operational and metal transfer, influencing the geometry, mechanical properties and metallurgical characteristics of the weld. The thermal conductivity of each shielding gas directly influences the fusion efficiency. Figure 3 compares the thermal conductivity for argon, helium and mixtures between them, observing that for temperatures above 15,000 K the thermal conductivity of helium increases considerably compared to argon. Argon at atmospheric pressure and at 20,000 K of temperature has a thermal conductivity close to 2.64 J/m s K, while pure helium at same conditions has a thermal conductivity of 40 J/m s K (Ref 32). Therefore, helium has a higher heat transfer capacity resulting in a higher heat

imposed on the base metal, facilitating the welding of materials with high thermal conductivity and enabling the use of higher welding speeds. Compared to argon, helium forms larger and rounder weld beads in the MIG process, however not necessarily with greater penetration (Ref 33).

Aim of the Investigation

The objective of this article is to study the behavior of gray cast iron with lamellar graphite, using duplex stainless steel as filler material, and observe the crack behavior on the weld beads. The MIG-CMT and PTA-P welding processes will be used. The welding parameters for each welding process will be adjusted according to the requirements of each process to obtain the best weld quality. Therefore, parameters such as amplitude of oscillation and welding speed will be adjusted. Different preheating temperatures

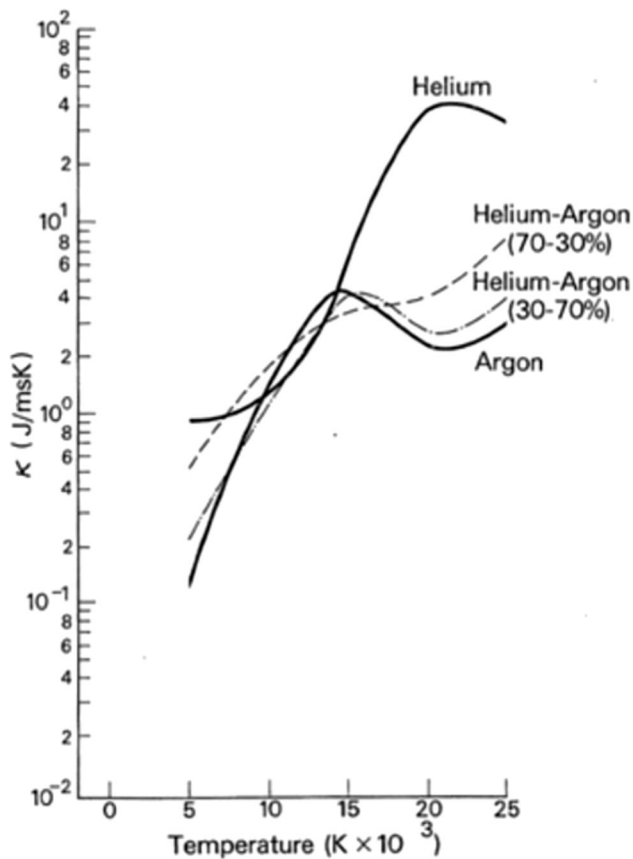


Fig. 3 Thermal conductivity of inert gases at 1 atm pressure. Adapted from (Ref 32)

will be applied, in order to observe their impact on the behavior of the cracks and the chemical composition of the weld beads. As shielding gases, mixtures of argon with different helium amounts will be studied, in order to observe their influence on the geometry of the weld beads and on the cracks of the base material, especially its influence on the dilution.

Materials and Experimental Details

Material

The filler material used for the MIG process was a duplex stainless steel solid wire G 22 9 3 N L (EN ISO 14343-A) of 1.0 mm diameter. The powder used as filler material for the PTA-P process was manufactured by gas atomization and with a granulometry between -150 and $+53$ μm and has a composition within the limits of a duplex stainless steel 1.4462 (EN 10088-3) (Fig. 4). The base material used is an EN-GJL-250 gray cast iron plate with dimensions of 300 mm \times 200 mm \times 8 mm ($w \times b \times t$). The chemical

composition of the materials is determined by spark optical emission spectroscopy (Table 1).

The MIG welding power source used within the experiments was a Fronius Cold Metal Transfer Advanced 4000, with the synergic curve for CrNi 19 9 (CMT 0877), whereas the plasma-transferred arc welding source used was a Castolin Eutectic Eutronic GAP 2501. A set of standard parameters, with the aim of achieving a low dilution level, was determined experimentally for both processes (Table 2). A data acquisition system with 20 kHz acquisition rate was used to measure the voltage and current signals of the arc welding processes; furthermore, three thermocouples were attached (in 5 mm distance of each other) next to the weld bead flank (5 mm) to obtain the temperatures and cooling rates of the weld beads (Fig. 5). The cooling rate was defined as the rate of change ($^{\circ}\text{C}/\text{min}$) necessary to reach a temperature 50 $^{\circ}\text{C}$ lower than the maximum temperature of each measurement made with the thermocouple 1.

In order to study the influence of the preheating on the formation of the microstructures and the dilution level, the cast iron plates were clamped on a heater plate. The surfacing layers were made at room temperature (25 $^{\circ}\text{C}$) and at preheating temperatures of 200 and 400 $^{\circ}\text{C}$. Three different types of shielding gas were used and each one with different helium amounts of 0, 30 and 100%, with the objective of observing its influence on the geometry and the superficial cracks of the weld bead.

Methods

Before carrying out the welding tests, the surface of the base materials was ground to remove any surface oxide. Then, the surface was cleaned with ethanol to remove any oil or polluting agent. Single weld beads were made to study the influence of each variable previously proposed.

To compare the influences of different gas mixtures, the parameters of each welding process were regulated in such a way that the energy of the arc was the same for each gas mixture.

The samples for the metallographic examination were obtained by cutting with a water jet process, trying to reduce the thermal influence of the cut on the microstructure of the sample. Standard metallographic procedure was used for microstructural examinations. Nital 2% solution was used to reveal various microstructure constituents in the weldment.

The composition of the weld beads was measured by removing 0.15 mm from the surface of the beads and analyzed by means of optical emission spectrometry (OES).

The average hardness of various microstructural zones in the weldments was obtained by Vickers microhardness test, specifically HV0.5 following DIN EN ISO 6507-1 and DIN EN ISO 9015-2.

Fig. 4 Morphology of powder used as filler material for the PTA-P process (1.4462)

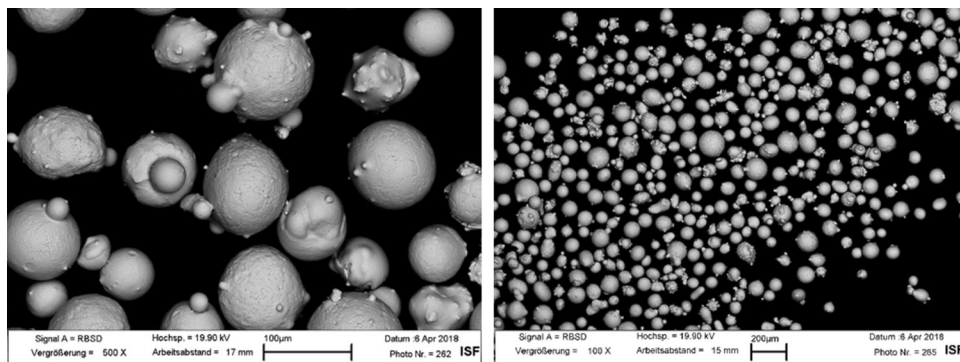


Table 1 Chemical composition by weight of gray cast iron EN-GJL-250 (EN 1561), duplex stainless steel wire (EN ISO 14343-A) and powder (EN 10088-3)

Material	C, wt.%	Mn, wt.%	Cr, wt.%	Mo, wt.%	Ni, wt.%	N, wt.%	Fe, wt.%
EN-GJL-250	3.43	0.760	0.110	0.040	0.100	...	92.0
Duplex stainless steel (wire)	0.024	1.77	21.6	3.13	5.73	0.158	66.7
Duplex stainless steel (powder)	0.029	1.20	23.42	3.22	5.66	...	65.3

Table 2 Welding variables and parameters

	MIG-CMT	PTA
Welding speed, cm/min	40	5
Wire feeding rate, m/min	7	...
Powder feeding rate, kg/h	...	1.4
Shielding gas, L/min	20	15
Plasma gas, L/min	...	0.5
Feeding gas, L/min	...	3.0
Correction, %	+15	...
Torch inclination angle, °	+15 (stabbing)	0
Distance contact tube, mm	14	5
Preheat temperature, °C	25, 400	25, 200, 400
Shielding gas type	Ar, ArHe30, He	Ar, ArHe30, He
Plasma gas type	...	Ar
Feeding gas type	...	Ar, ArHe30, He
Constrictor nozzle diameter, mm	...	2.6
Oscillation amplitude, mm	...	20
Oscillation frequency, Hz	...	1

Results

Metal Inert Gas (MIG) Welding Process by Cold Metal Transfer (CMT) on Gray Cast Iron

Influence of the Preheating Temperature

The cross sections of the weld beads did not reveal imperfections as internal porosities or cracks (Fig. 6). The geometries of the weld beads were strongly affected by the increase in the preheating temperature, especially the width

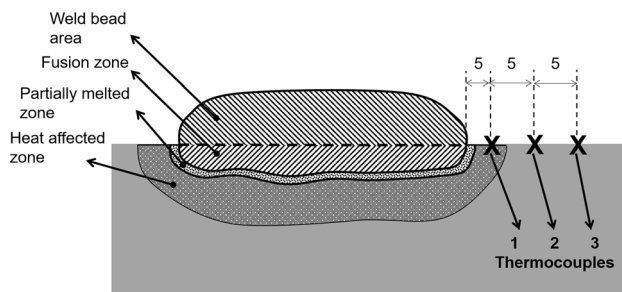


Fig. 5 Thermocouples distribution (1, 2, 3) and different zones that compound the weld bead

Fig. 6 Macrosections of weld beads (MIG-CMT process with argon as shielding gas) at preheating temperatures (a) 25 °C and (b) 400 °C

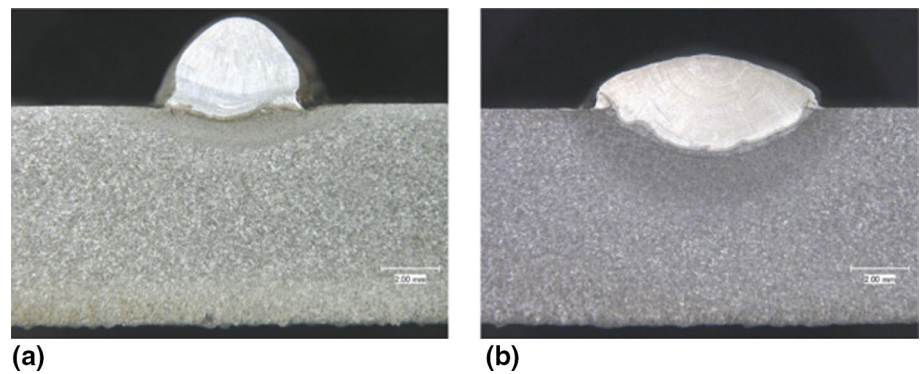
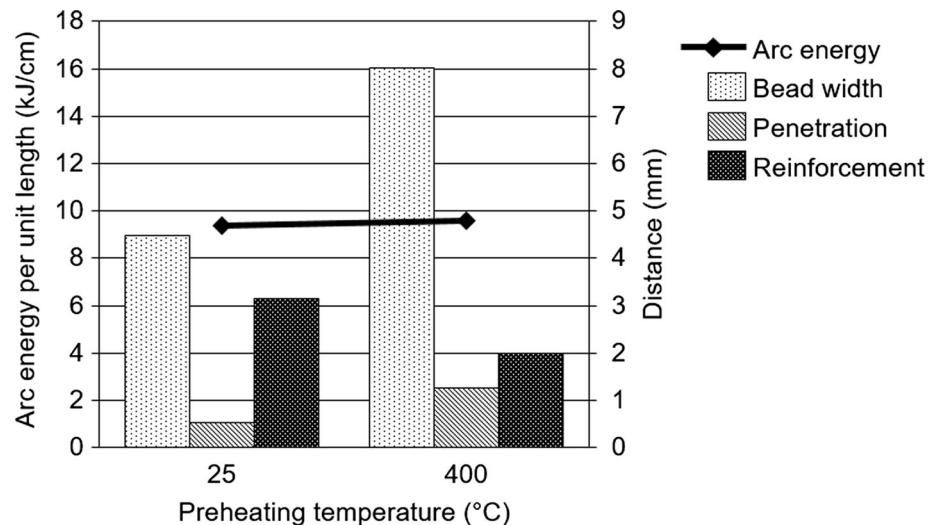


Fig. 7 Influence of the preheating temperature on the geometry of the weld beads considering the arc energy per unit length



of the weld beads, which increases from 4.5 to 8 mm (Fig. 7). The penetration and the reinforcement of the weld bead were also affected, and both varied around 1 mm, the penetration increased, and the bead height decreased. The arc energy per unit length remained practically constant during the tests.

The fusion zone (FZ) has a behavior similar to penetration and weld bead height, increasing while the bead area has no significant changes (Fig. 8). The dilution at room temperature is 8.9%, while with preheating temperature of 400 °C the dilution is 20.4%. On the other hand, the area of the PMZ also increases with the preheating temperature, starting with 0.8 mm² until reaching 1.2 mm². The hardness in the PMZ increased approximately 80 HV0.5 when the preheating temperature was 400 °C. However, the HAZ had a greater change in its hardness, starting with 658 HV0.5 for room temperature and with 361 HV0.5 for 400 °C with preheating (Fig. 9). These changes in the PMZ and the HAZ are visible in Fig. 10, where a large change in the HAZ is observed for 400 °C preheating temperature.

Influence of the Helium Amount in the Shielding Gas

The amount of helium in the shielding gas directly influenced the geometry of the weld beads and the penetration profile, observing a type of “finger shape” profile for 100% helium (Fig. 11). Furthermore, the weld beads made with 30 and 100% of helium contents showed some superficial cracks, as observed in Fig. 11(d). The width of the weld beads increased as the amount of helium increased in the shielding gas, beginning with 4.5 mm for pure argon to 9.8 mm for 100% helium. In the case of the penetration and reinforcement of the weld bead, its behavior is similar to that observed in the tests for different preheating temperatures (Fig. 12).

The dilution increased to a level similar to that achieved for a preheating of 400 °C, in this case a maximum of 19.3%. The FZ consequently increased with the amount of helium. The area of the PMZ was increased with the largest amount of helium to approximately 1.3 mm² (Fig. 13). The maximum hardness measured in the PMZ for 100% helium was 622 HV0.5, a similar value for that obtained in the

Fig. 8 Influence of the preheating temperature on different zones and dilutions of the weld beads. MIG-CMT process with pure argon as shielding gas

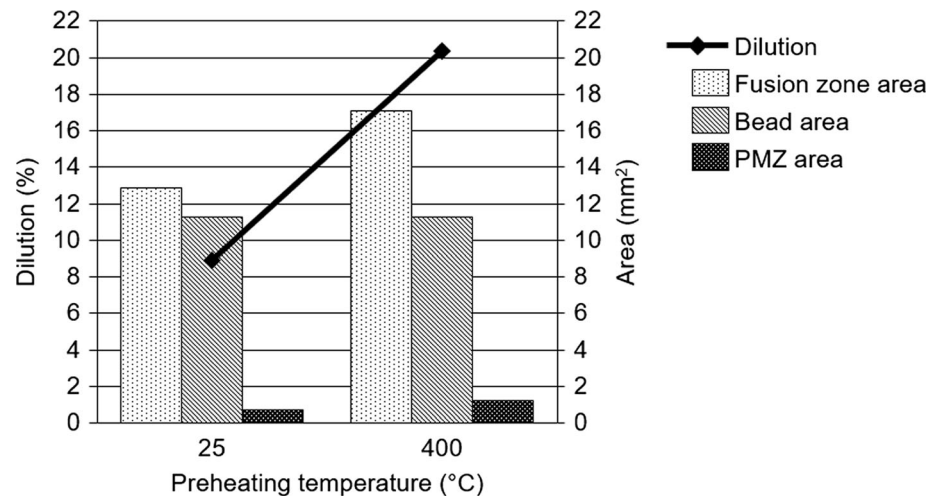
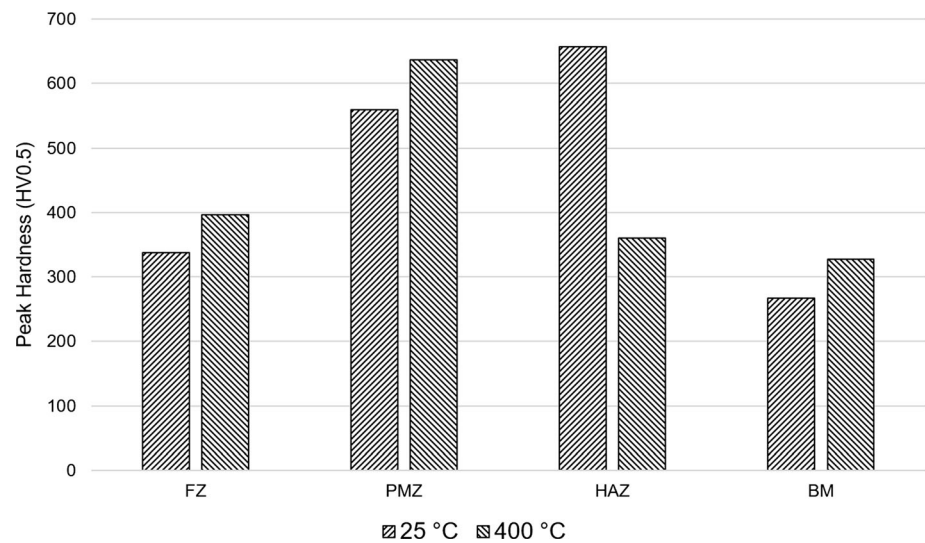


Fig. 9 Microhardness of different zones in the weld bead for different preheating temperatures. MIG-CMT process with pure argon as shielding gas



same zone for 400 °C of preheating, approximately 637 HV0.5. However, the behavior of the HAZ is totally different if compared to the behavior for preheating; in this case, the HAZ becomes harder for higher helium contents in the shielding gas, reaching a maximum hardness of 661 HV0.5 (Fig. 14).

Plasma-Transferred Arc Powder (PTA-P) Welding on Gray Cast Iron

Influence of the Preheating Temperature

No cracks and porosities are observed in any of the areas of the weld bead in the cross sections of the weld beads made for three levels of preheating temperature (Fig. 15). The width and penetration of the weld beads did not show

significant variations, while the arc energy per unit length remained without relevant variations (Fig. 16).

The preheating temperature had a significant influence on the penetration, which varied between 0.4 mm (25 °C) and 0.7 mm (400 °C). The width of the weld beads varied between 24.5 mm (25 °C) and 24.8 mm (400 °C), while the weld bead reinforcement tended to decrease strongly, obtaining 3.4 mm (25 °C) and 2.6 mm (400 °C) (Fig. 16). This behavior in the reinforcement is explained by the increase in the FZ and the decrease in the area of the weld bead, which also causes the increase in dilution up to 21% (400 °C) (Fig. 17). The increase in the preheating temperature also favored the growth of the PMZ area, which at 25 °C is 5.3 mm², while at 400 °C it is 8.7 mm².

The influence of the preheating temperature, in addition to influencing the growth of the PMZ, also influenced the

Fig. 10 Microhardness measurements for the samples made with MIG-CMT process with 25 and 400 °C preheating temperature

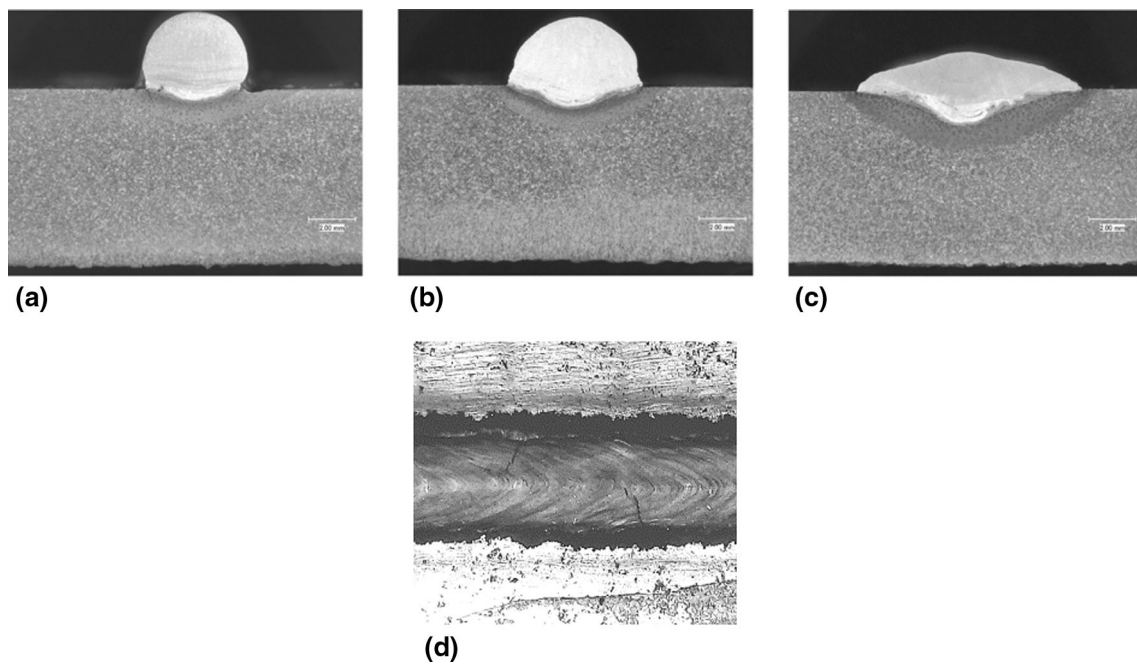
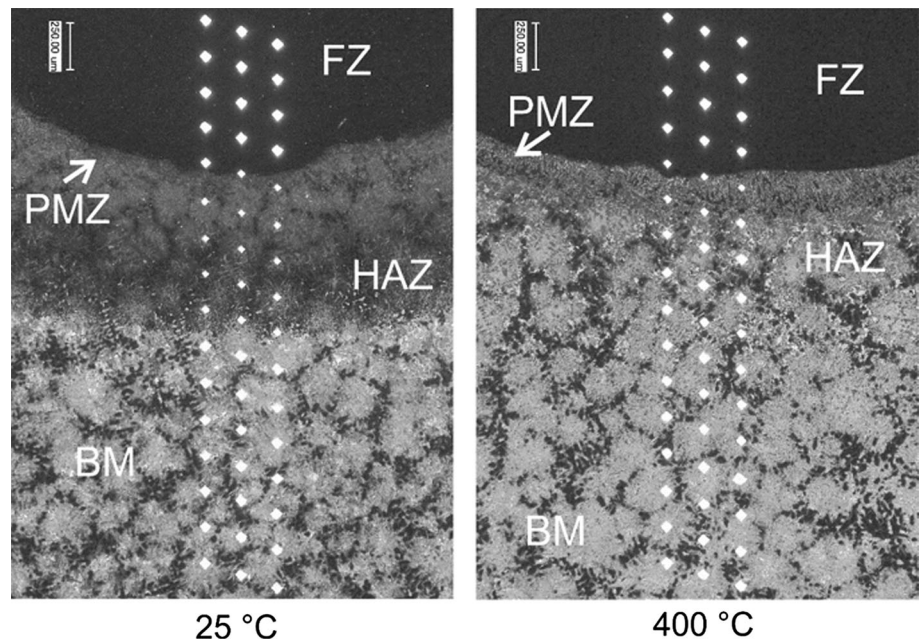


Fig. 11 Macrosections for different helium amounts in the shielding gas (a) 0%, (b) 30%, (c) 100%, (d) superficial appearance of the single weld bead with 100% of helium content. MIG-CMT process without preheating

increase in hardness, whereas for temperatures of 25 and 200 °C the hardness of the PMZ remained without significant changes, around 520 HV0.5, while for 400 °C the hardness increased drastically to 670 HV0.5. On the other hand, the hardness of the HAZ tends to decrease with the increase in the preheating temperature, reaching a minimum value of 291 HV0.5 for 400 °C. The fusion zone tends to increase its hardness with the preheating

temperature, from 242 HV0.5 (25°) to 307 HV0.5 (400 °C) (Fig. 18).

Influence of the Helium Amount

The cross sections of the weld beads did not show internal cracks; however, when pure helium is used as shielding and feeding gas, internal porosities can be observed (Fig. 19).

Fig. 12 Influence of the helium amount in the shielding gas on the penetration, width and reinforcement of the weld beads considering the arc energy per unit length. MIG-CMT process without preheating

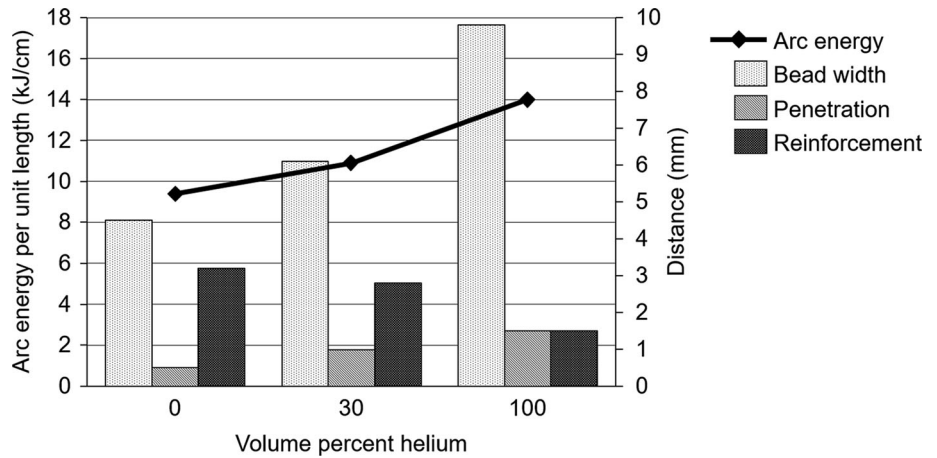


Fig. 13 Influence of the helium amount in the shielding on different zones and dilutions of the weld beads. MIG-CMT process without preheating

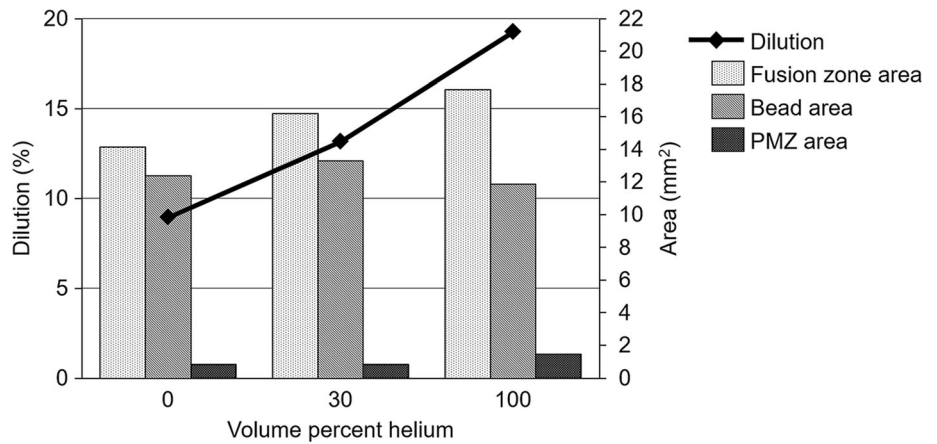
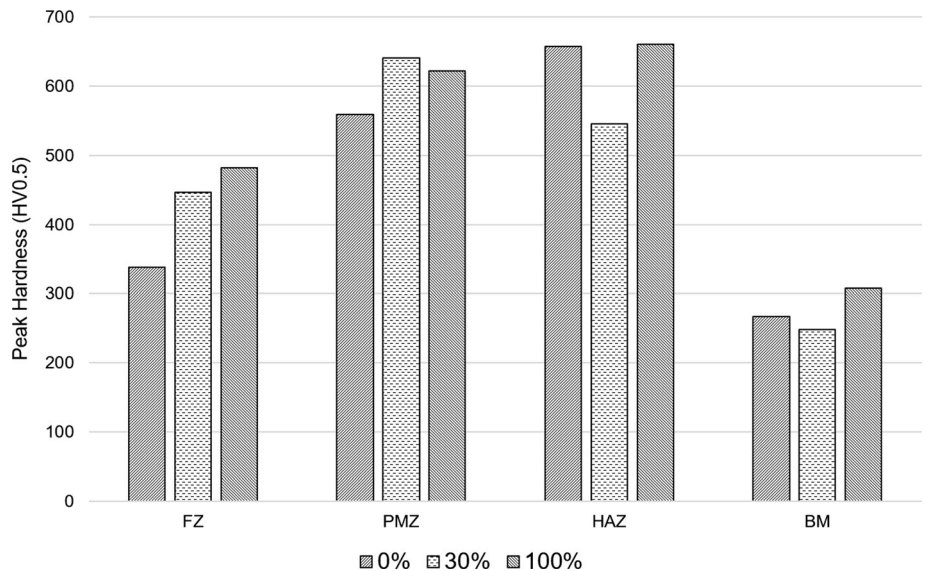


Fig. 14 Microhardness of different zones in the weld bead for different amounts of helium. MIG-CMT process without preheating



In comparison with welds made with pure argon, helium had a greater influence on the width of the weld bead. Also, a variation is observed in the penetration (Fig. 20). With helium amounts lower than 30%, there are no significant

differences in the width of the weld bead. When 100% helium is used, the width of the weld bead increases to 28 mm. In the case of the penetration and reinforcement of the weld bead, both have an opposite behavior. While the

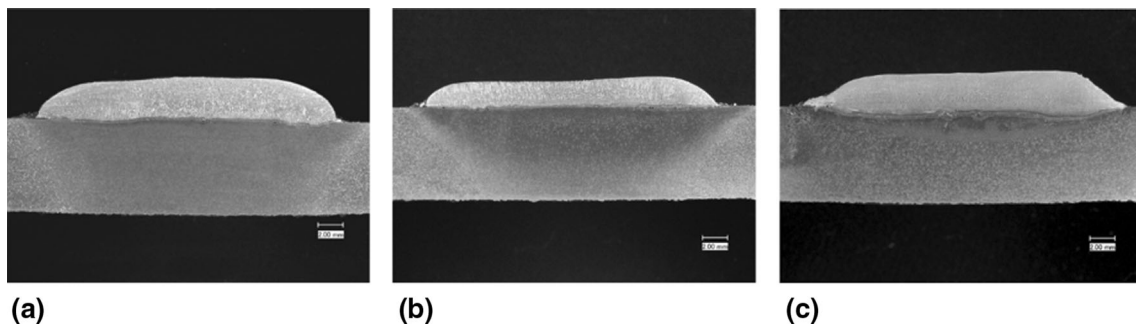


Fig. 15 Macrosections for different preheating temperatures (a) 25 °C, (b) 200 °C, (c) 400 °C. PTA-P process with argon as plasma gas and shielding gas

Fig. 16 Influence of the preheating temperature on the penetration, width and reinforcement of the weld beads considering the arc energy per unit length during the welding process. PTA-P process with argon as plasma gas and shielding gas

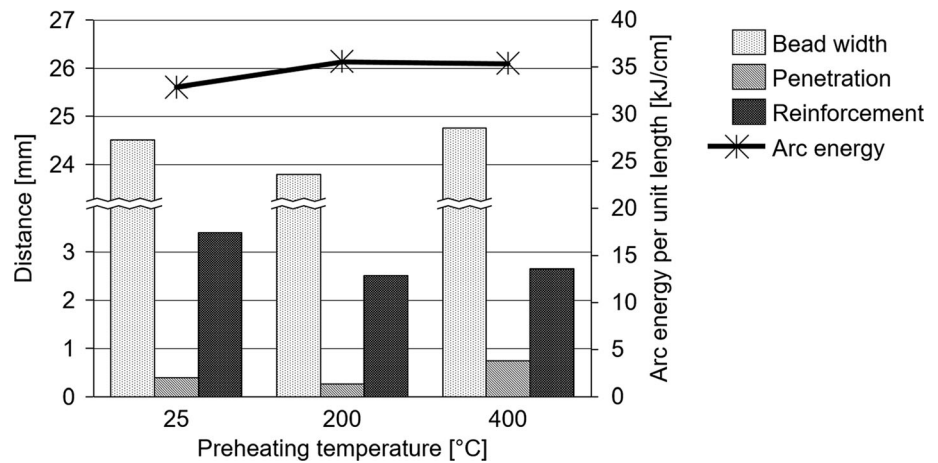
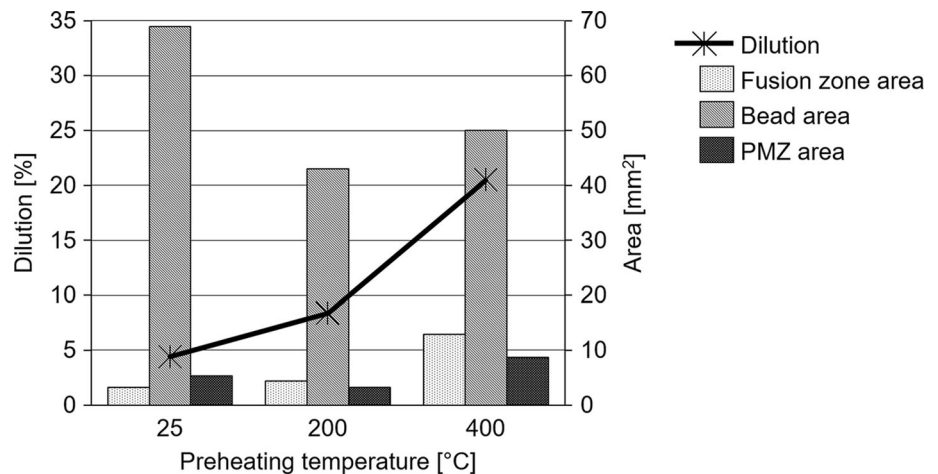


Fig. 17 Influence of the preheating temperature on different zones and dilutions of the weld beads. PTA-P process with argon as plasma gas and shielding gas



penetration increases from 0.4 to 1.3 mm with the amount of helium, the reinforcement decreases from 3.4 to 1.6 mm. As in the MIG-CMT process, when increasing the helium content in the shielding gas, cracks were observed on the surface (Fig. 19d).

The dilution of the weld beads changed from 4.4 to 36% when the amount of helium increased in the shielding gas. This is supported by the progressive decrease in the weld bead area and the increase in the fusion zone, indicating

that there is a greater dilution between the filler material and the base material (Fig. 21). However, PMZ tended to reduce its size when the amount of helium increased, from 5.3 mm² for pure argon to 4 mm² for pure helium, while its hardness increased with the amount of helium present in the shielding gas. Similar behavior had the hardness in the fusion zone and the HAZ; it increased with the amount of helium in the shielding gas (Fig. 22).

Fig. 18 Microhardness of different zones in the weld bead for different preheating temperatures. PTA-P process with argon as plasma gas and shielding gas

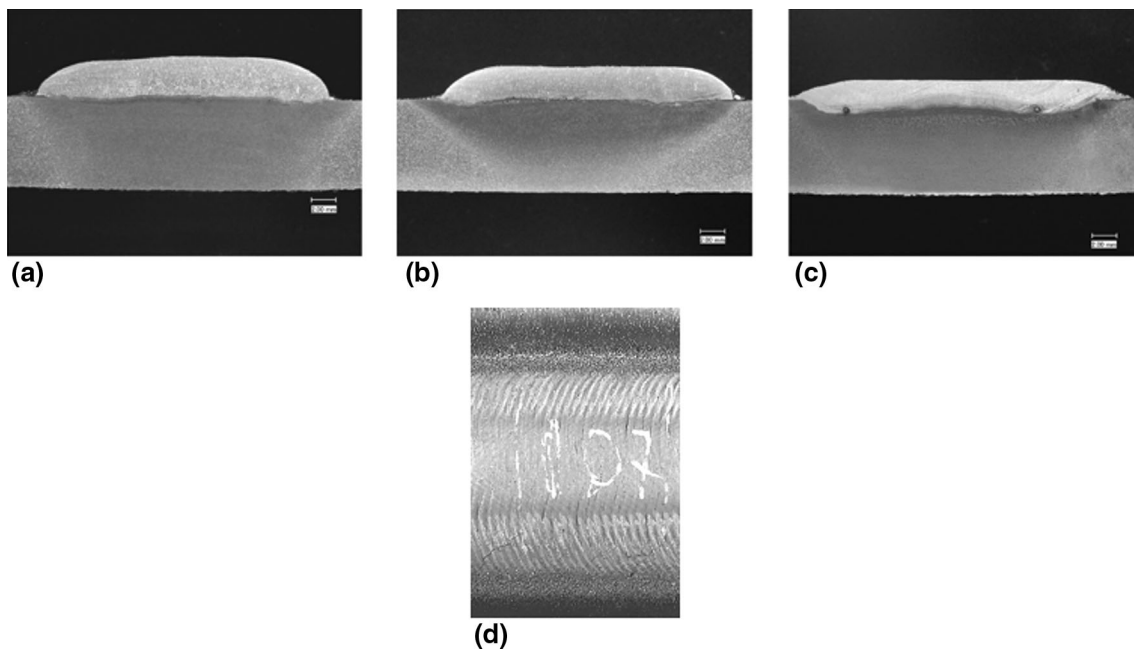
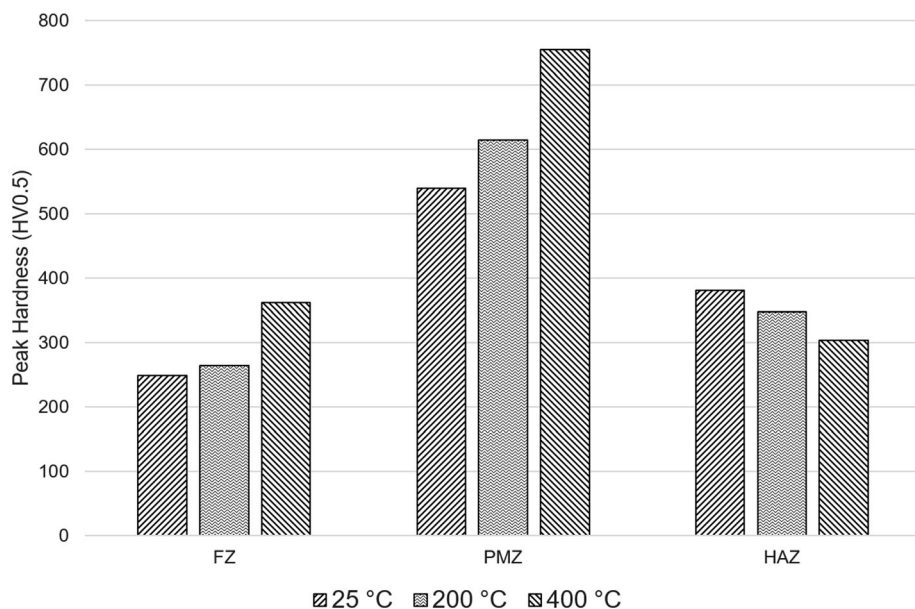


Fig. 19 Macrosections for different helium amounts in the shielding and feeding gas (a) 0%, (b) 30%, (c) 100%, (d) superficial appearance of the single weld bead with 100% of helium content. PTA-P process without preheating

Discussion

From the analysis made to the geometry of the weld beads, it was observed that the penetration behavior and the bead width, in the specific case of the MIG-CMT process, were strongly affected, enlarging the width of the weld bead and the penetration when the amount of helium and the preheating temperature were increased. When the preheating temperature increased, the width and penetration rose due to the fact that the base material was already at an elevated

temperature (400 °C), which facilitated the formation of the melted pool and the melting of the base material, achieving greater penetration and bead width. In the case of the increase in the amount of helium in the shielding gas, the bead width and penetration were increased by the increase in the arc energy, product of the high ionization potential required by helium, which rise the welding arc temperature, promoting an increase in the width and penetration.

Fig. 20 Influence of the helium amount in the shielding and feeding gas on the penetration, width and reinforcement of the weld beads. PTA-P process without preheating

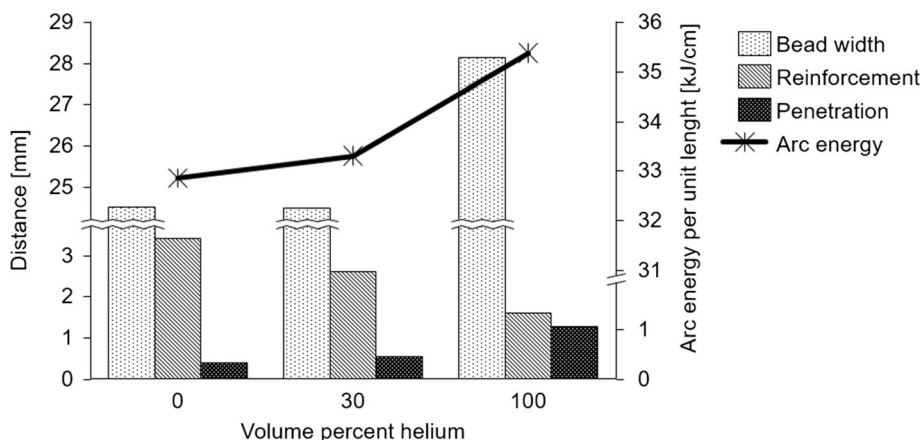
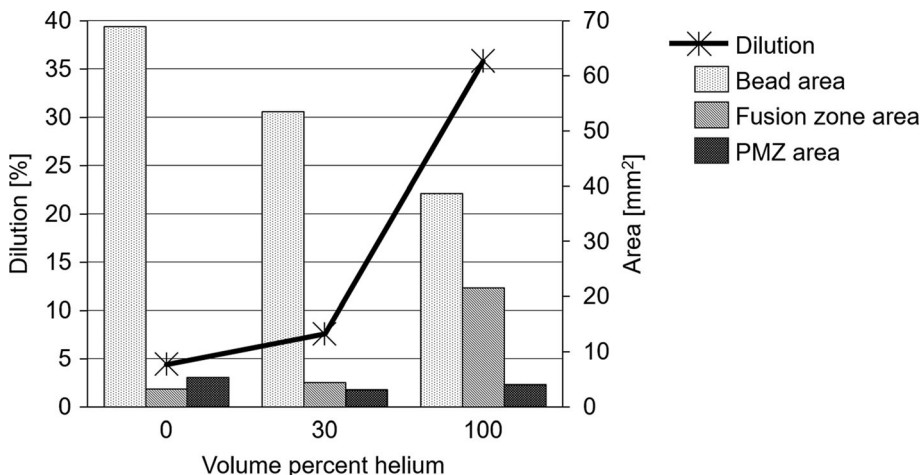


Fig. 21 Influence of the helium amount in the shielding and feeding gas on different zones and dilutions of the weld beads. PTA-P process without preheating



Filler material in PTA-P process is added externally, interposing between the molten pool and the welding arc, leading to the arc energy being used as a great part to melt the additional material and not the base material, influencing the penetration depth. The bead width obtained by the PTA-P process was influenced significantly just when the amount of helium increased in the shielding gas; this is due to the increase in the arc energy, as it happened with the MIG-CMT process.

By increasing the preheating temperature or the amount of helium in the shielding gas, different areas that compound the weld bead were affected. The fusion zone (FZ) was significantly affected; in particular, the MIG-CMT

process had a bigger FZ than the PTA-P, which makes sense when the penetrations and the bead areas are compared for both welding processes. The size of the FZ depends on the time during which the base metal remains above the melting point (Ref 34). This time is prolonged when the base metal is preheated. Therefore, it is expected that when the preheating temperature increases, consequently the bead width, penetration and FZ increase also, having a tendency to prevent the formation of martensite. Other investigations show opposite results, where the weld beads were thinner (Ref 13). Figure 23(a) shows the temperature curves for weld beads made with PTA-P process with pure argon and the mixture argon with 30% of helium

Fig. 22 Microhardness of different zones in the weld bead for different amounts of helium. PTA-P process without preheating

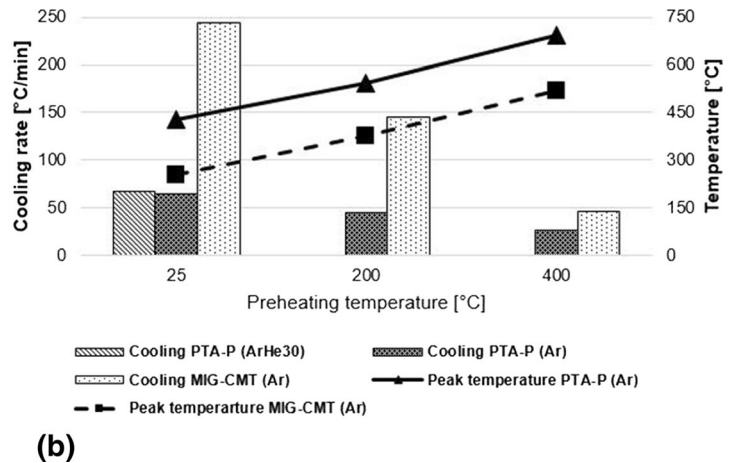
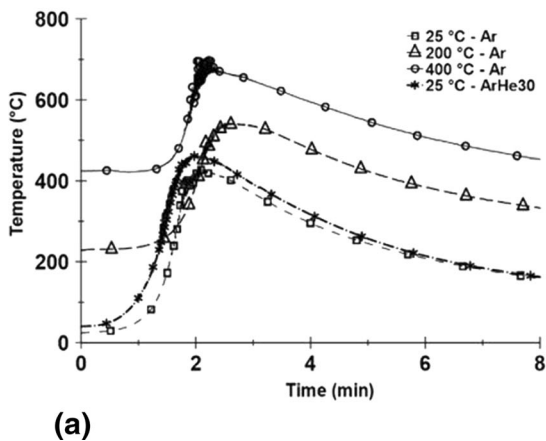
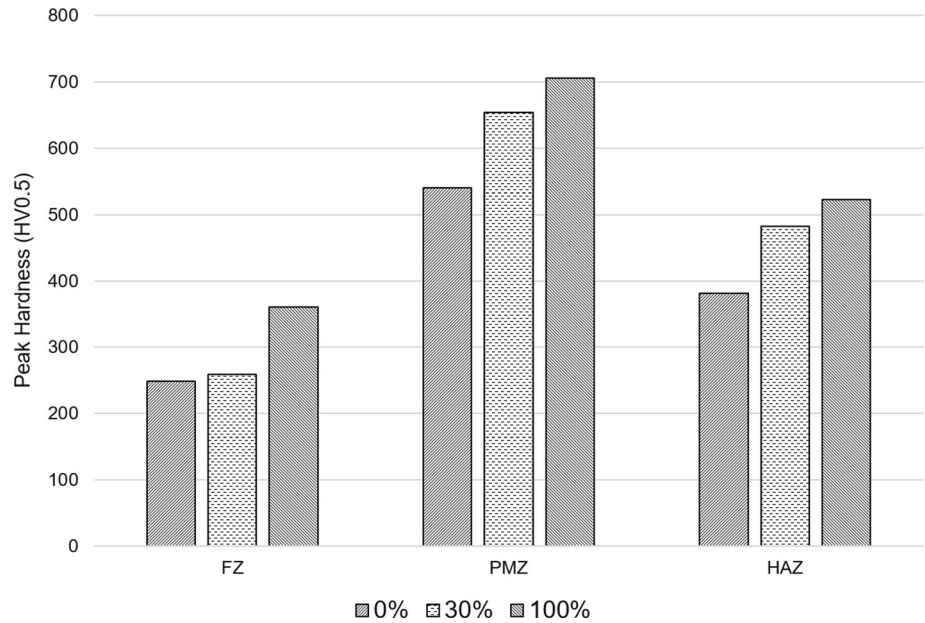


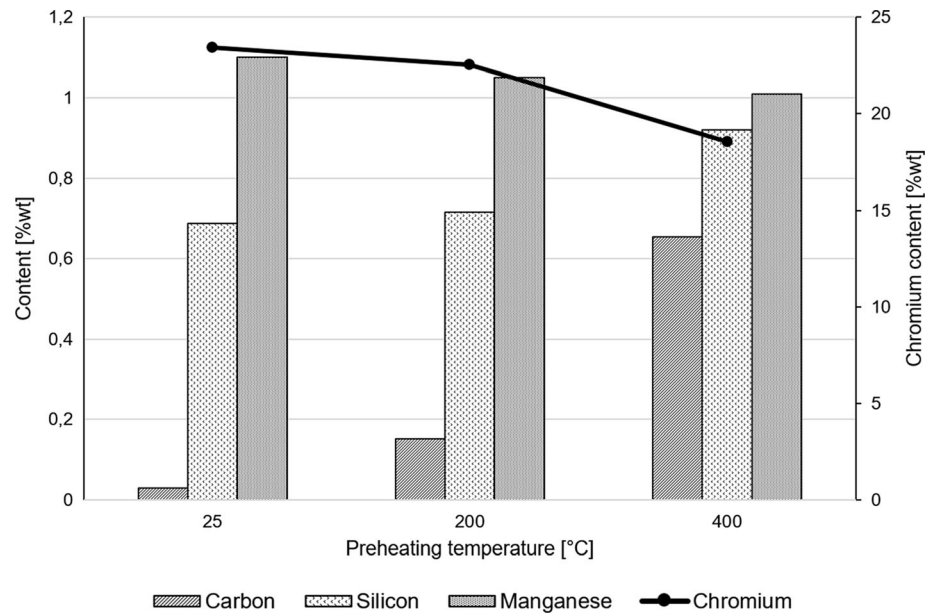
Fig. 23 (a) Temperature curves and (b) cooling rate values for different preheating temperatures and shielding gases in the PTA-P and MIG-CMT processes

as shielding gas for 25 °C of preheating temperature, noticing that temperature at which the weld bead is exposed is greater with the mixture gas. Furthermore, in Fig. 23(a) are presented cooling curves for different preheating temperatures with pure argon as shielding gas, observing as the preheating temperature increases, the weld bead is exposed to higher temperatures and for a longer period of time. Figure 23(b) shows how the cooling rates decrease while the preheating temperature grows up, which means that at a higher preheating temperature the weld bead cools more slowly. This last result is important for its

influence on the weld bead hardness because as observed in microhardness measurements, with slower cooling, higher final hardness in the FZ and PMZ was obtained in the weld bead.

The hardness of different zones was also analyzed, finding that the PMZ is the one that has the highest hardness. El-Banna (Ref 13) mentioned that the carbide precipitation is responsible for the high values of the hardness in the PMZ. In the same work, the hardness of all zones (FZ, PMZ, HAZ) decreased when the preheating temperature increased to 300 °C. According to the results

Fig. 24 Chemical composition of fusion zone for the PTA-P samples for different preheating temperatures obtained by optical emission spectrometry (OES)



obtained in the present article, when preheating was used, the HAZ decreased its hardness, while the FZ and PMZ had the tendency to increase its value, in both welding processes. Comparing the hardness of the FZ between the PTA-P process and the MIG-CMT, the latter has higher values; however, in the PMZ the hardness values of the PTA-P process are highest for 400 °C of preheating. In the case of the tests carried out for different amounts of helium in the shielding gas, the microhardness in all the zones had the tendency to increase, and it is highlighted that in the specific case of the MIG-CMT process, the hardness of the HAZ was greater than the PMZ. In Fig. 24, the chemical composition measured in the weld beads made by PTA-P process with pure argon for different preheating temperatures is observed, where it is noticed how increasing the temperature increases the amount of carbon in the FZ, while the amount of chromium decreases. This agrees with (Ref 13, 14, 21, 34) and with the results shown in Fig. 17, where the dilution level of the weld beads for 400 °C of preheating was 20.5%. Comparing the hardness of the HAZ of the tests carried out with preheating and those with different amounts of helium, it is observed that the hardness is greater for the tests with different amounts of helium in both processes. The reason is that the cooling rate without preheating and additional helium in the shielding gas is greater (68 °C/min for PTA-P) which according to (Ref 14, 34) would promote the formation of hard and brittle microstructures in the HAZ.

Comparing the cooling rates of each welding process when preheating is used, it is possible to understand the

differences in HAZ hardness. In the case of the PTA-P process without preheating, the cooling rate was approximately 64.4 °C/min, while for the MIG-CMT process it was 244 °C/min. This difference is mainly due to the high arc energy used in the PTA-P process in comparison with MIG-CMT. With these cooling rates, the peak hardness in the HAZ of the weld beads made with the PTA-P was 381.5 HV0.5, while the MIG-CMT process reached 657.6 HV0.5. The tendency to reduce the hardness is similar when the preheating temperature was increased to 400 °C, 303 HV0.5 for PTA and 361 HV0.5 for MIG-CMT, where the cooling rates were 27.4 °C/min for PTA-P and 46 °C/min for MIG-CMT. The decrease in hardness is due to the fact of the decreasing the cooling rate when the preheating temperature is increased; therefore, it is expected a softer microstructure in the HAZ and not the hard and brittle martensite (Ref 35). Figure 25 shows how in the case of the MIG-CMT process the HAZ of the weld bead without preheating is mainly composed of martensite, while by increasing the preheating temperature to 400 °C the microstructure changed to a mainly ledeburite, which corroborates that was obtained with microhardness measurements. The high cooling rate of the MIG-CMT process is explained by the low energy per unit length (Fig. 7), where the value is approximately 10 kJ/cm compared to the PTA-P process that has an energy per unit length of 36 kJ/cm (Fig. 16). Therefore, the temperature reached by the base material with the MIG-CMT process is lower than that of the PTA-P process (Fig. 23(b)). Considering the known behavior of MIG processes in general, there is

Fig. 25 Comparison of different microstructures present in the HAZ for the MIG-CMT and PTA-P processes without preheating (25 °C) and with preheating of 400 °C

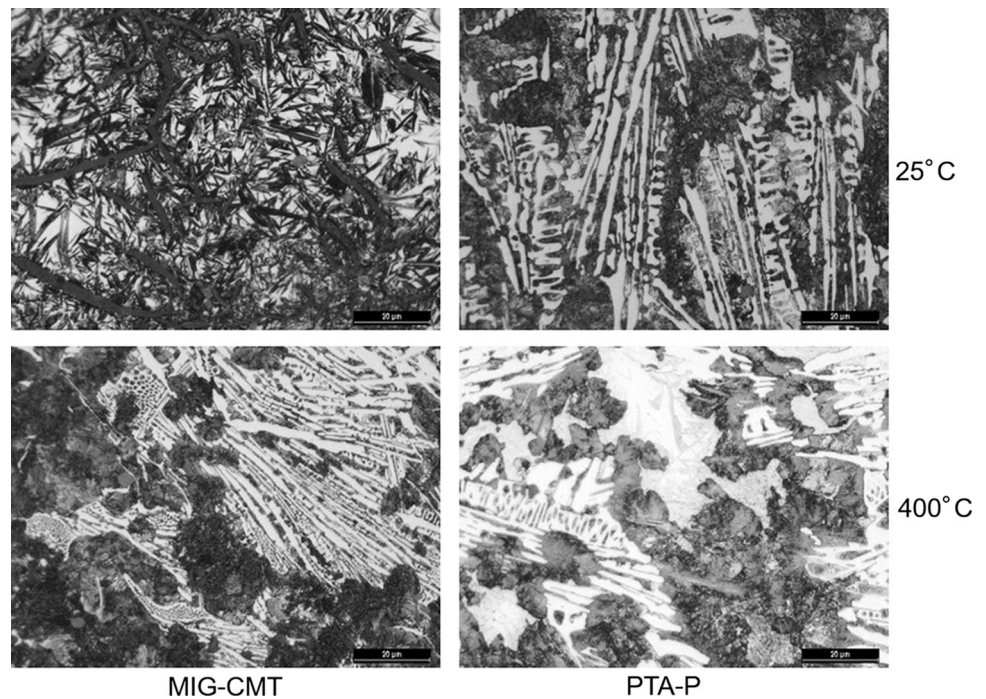
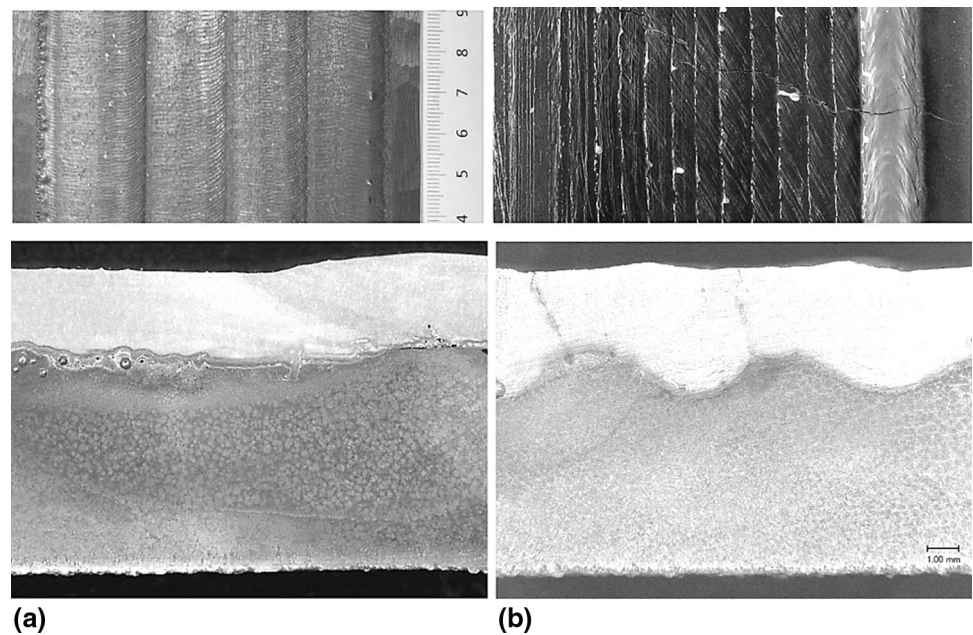


Fig. 26 Surface layers made by welding processes (a) PTA-P, (b) MIG-CMT with a preheating temperature of 400 °C



another possible explanation: Although the measured energy per unit length might be lower in comparison with PTA-P, the local heat input between PMZ and HAZ can be higher, resulting in higher local dilution and therefore in a higher carbon diffusion which leads to higher hardness due

to martensite content with similar cooling rates. This, however, requires further investigation.

The high hardness in the weld bead caused by the high cooling rate has a significant impact when consecutive weld beads are making to produce a surface layer.

Figure 26 shows a comparison between the surface layers made with a preheating temperature of 400 °C with the PTA-P and MIG-CMT processes, using the welding parameters described in Table 2. In the case of the surface layer made by the MIG-CMT process, a crack is evidenced on the surface, which crosses through all the weld beads that compound the surface layer. It should be noted that the crack is formed during the cooling of the surface layer. The surface layer made with the PTA-P process did not present cracks or any other type of defect on the surface layer. The defects observed in the surface layer made by the MIG-CMT process can be explained by the rapid rate of cooling (Fig. 23) which causes a high degree of hardness in the PMZ (Fig. 9).

Conclusions

According to the results reported in this work, it can be stated that:

1. The width and the penetration of the weld beads made by the PTA-P process were influenced when the preheating temperature and the helium content in the shielding gas were increased. However, the welds made by the MIG-CMT process had a strong increase in their penetration and width when the preheating temperature or the amount of helium in the shielding gas increased.
2. The increase in the preheating temperature and the amount of helium in the shielding gas promoted the growth of the FZ and the PMZ, especially in the MIG-CMT process.
3. The MIG-CMT process obtained higher hardness values in all the tests carried out, due to higher dilution percentages that mean an important diffusion of carbon toward to weld bead.
4. The PTA-P process obtained the lowest dilution (4.4%) at room temperature, even though the arc energy was greater than that of the CMT process. However, when both processes worked with 400 °C, their dilutions were approximately similar, 20%.
5. While the preheating temperature increased, the dilution increased, and consequently, the hardness of the FZ and the PMZ raised, while the hardness of the HAZ decreased due to the lower cooling rates with the PTA-P process. Similar hardness behavior was observed when the amount of helium increased in the shielding gas; however, in this case, the hardness of the HAZ was not reduced with the increase in helium.
6. The PTA-P process proved to be better than the MIG-CMT process when used on gray cast iron. However,

the operational complexity of the PTA-P process makes the MIG-CMT a viable option when a decision must be made.

Acknowledgment Open Access funding provided by Projekt DEAL. This work was supported by the DFG (Deutsche Forschungsgemeinschaft) (reference number RE 2755/41-1) and “Becas Chile” scholarship by the National Commission for Scientific and Technological Research (CONICYT). The authors wish to express their grateful acknowledgement for the support.

Open Access This article is licensed under a Creative Commons Attribution 4.0 International License, which permits use, sharing, adaptation, distribution and reproduction in any medium or format, as long as you give appropriate credit to the original author(s) and the source, provide a link to the Creative Commons licence, and indicate if changes were made. The images or other third party material in this article are included in the article’s Creative Commons licence, unless indicated otherwise in a credit line to the material. If material is not included in the article’s Creative Commons licence and your intended use is not permitted by statutory regulation or exceeds the permitted use, you will need to obtain permission directly from the copyright holder. To view a copy of this licence, visit <http://creativecommons.org/licenses/by/4.0/>.

References

1. K. Yıldızlı, M.B. Karamış, and F. Nair, Erosion Mechanisms of Nodular and Gray Cast Irons at Different Impact Angles, *Wear*, 2006, **261**(5-6), p 622-633
2. W.J. Tomlinson and M.G. Talks, Erosion and Corrosion of Cast Iron Under Cavitation Conditions, *Tribol. Int.*, 1991, **24**(2), p 67-75
3. G. Pintaude, F.G. Bernardes, M.M. Santos, A. Sinatora, and E. Albertin, Mild and Severe Wear of Steels and Cast Irons in Sliding Abrasion, *Wear*, 2009, **267**(1-4), p 19-25
4. Federal-Mogul, Pvd-Laufflächenbeschichtung Von Guss-Kolbenringen (Pvd-Coating of Treads of Cast Cylinder Rings), *MTZ*, 2008, **06**(2008), p 478
5. S. Zhuo, Z. Peijun, Z. Leheng, X. Xinfu, H. Aimin, and Z. Wenquan, Multi-Layer Compound Coating on Cast Iron Piston Ring By Multi-Arc and Magnetron Sputtering Ion Compound Plating Technique, *Surf. Coat. Technol.*, 2000, **131**(1-3), p 422-427
6. J.-J. Jeong, B.-Y. Jeong, M.-H. Kim, and C. Lee, Characterization of Tin Coatings on the Plasma Nitrided Spheroidal Graphitic Previous Termcast Iron Substrates, *Surf. Coat. Technol.*, 2002, **202**, p 24
7. T. Irisawa and H. Matsumoto, Thermal Shock Resistance and Adhesion Strength of Plasma-Sprayed Alumina Coating on Cast Iron, *Thin Solid Films*, 2006, **509**(1-2), p 141-144
8. O. Maranhão, D. Rodrigues, M. Boccalini, and A. Sinatora, Influence of Parameters of the HVOF Thermal Spray Process on the Properties of Multicomponent White Cast Iron Coatings, *Surf. Coat. Technol.*, 2008, **202**(15), p 3494-3500
9. V. Ocelík, U. de Oliveira, M. de Boer, and J.T.M. de Hosson, Thick Co-Based Coating on Cast Iron By Side Laser Cladding: Analysis of Processing Conditions and Coating Properties, *Surf. Coat. Technol.*, 2007, **201**(12), p 5875-5883
10. D.T. Gawne, Failure of Electrodeposited Chromium Coatings on Cast Iron Substrates, *Thin Solid Films*, 1984, **118**(3), p 385-393

11. L. Giordano, A. Tiziani, A. Zambon, and N. Antolotti, Characterization of Surface Chromium and Molybdenum Alloying on Gray Cast Iron Obtained By the Plasma-Transferred Arc Technique, *Mater. Sci. Eng., A*, 1991, **140**, p 727-732
12. L.B.P. Romvari, Herstellung Korrosionsbeständiger Schichten an Gusseisenwerkstoffen Aus Ferrit-Kugelgraphit (Production of Corrosive Resistant Coatings on Cast Iron Materials With Ferrite-Spherical Graphite), *Schweisstechnik*, 1990, **1990**, p 144-146
13. E.M. El-Banna, Effect of Preheat on Welding of Ductile Cast Iron, *Mater. Lett.*, 1999, **41**(1), p 20-26
14. M. Pouranvari, On the Weldability of Grey Cast Iron Using Nickel Based Filler Metal, *Mater. Des.*, 2010, **31**(7), p 3253-3258
15. F. Malek Ghaini, M. Ebrahimnia, and S. Gholizade, Characteristics of Cracks in Heat Affected Zone of Ductile Cast Iron in Powder Welding Process, *Engineering Failure Analysis*, 2011, **18**(1), p 47-51.
16. U. Szieslo and O. Penning, Auftragschweißen an Gußeisenwerkstoffen: (clad welding on cast irons innovative welding technologies) in DVS Berichte, *Innovative Schweißtechnologien*, 1998, **1998**, p 92-97
17. R.L. Kumar, Welding Grey Iron With Mild Steel Electrodes, *Foundry*, 1968, **96**(1), p 64.
18. A. Klimpel, 2003, Pulverauftragschweißen an Legiertem Gusseisen Mit Kugelgraphit (Pta-Cladding on Cast Iron With Spherical Graphite), *Schweißen und Schneiden*, 2003, **424**(426-428), p 430-431
19. P.A. Tyvonchuk, V.N. Naumenko, and M.A. Vasilenko, Arc Deposition of Steel on Cast Iron in Natural Gas, *Weld. Int.*, 1988, **2**(9), p 794-795
20. S. Chatterjee and T.K. Pal, Solid Particle Erosion Behaviour of Hardfacing Deposits on Cast Iron—Influence of Deposit Microstructure and Erodent Particles, *Wear*, 2006, **261**(10), p 1069-1079
21. J.R. Davis, Stainless Steel Cladding and Weld Overlays, *ASM Specialty Handbook: Stainless Steels*, 1994, **1994**, p 107-119
22. U. Reisgen, K. Willms, S. Wieland, E. Gonzalez, M. Oechsner, J. Ellermeier, M. Siebers, and B. Heider, Improving the Resistance of Grey Cast Iron Components By Cladding With Duplex Stainless Steel Using Controlled Gas Metal Arc Welding: Influence of Dilution on Corrosion Properties, *Mat.-wiss. u. Werkstofftech.* (in press).
23. U. Reisgen, M. Oechsner, R. Sharma, J. Ellermeier, G. Andersohn, T. Engler, E. Zokoll, E. Gonzalez, and B. Heider, Corrosion Resistance and Microstructure of Welded Duplex Stainless Steel Surface Layers on Gray Cast Iron, *Journal of Thermal Spray Technology*, (In press).
24. Fronius International GmbH, Current Welding Practice: Cmt Technology: Cold metal transfer - a new gas metal arc welding process, 2013rd ed., DVS Media, 2014.
25. J.C. Dutra, R.H.G.e. Silva, C. Marques, and A.B. Viviani, A New Approach For Mig/Mag Cladding With Inconel 625, *Weld World*, 2016, **60**(6), p 1201-1209.
26. H. Doren and K. Wernicke, Eds., Influence of the Welding Parameters in Plasma Arc Overlay Welding With Powders, 1985.
27. C.S. Hunt, "Plasma Transferred Arc (PTA) surfacing of small and medium scale components: a review", 1988.
28. R.L. Deuis, J.M. Yellup, and C. Subramanian, Metal-Matrix Composite Coatings By Pta Surfacing, *Composites Science and Technology*, 1998, **58**(2), p 299-309
29. V. Vergara, J. Dutra, and A.S. Climaco D'Oliveira, Hardfacing By Plasma Transferred Arc Process, Arc Welding, W. Sudnik, Ed., InTech, 2011.
30. Castolin, European Product Catalogue Welding Equipment.
31. U. Reisgen, Grundlagen Der Fügetechnik: Schweißen, Löten und Kleben, DVS Media GmbH, 2016, [2016.
32. J.F. Lancaster, Ed., The Physics of Welding, 2nd ed., Pergamon Press, 1986.
33. A. Scotti and V. Ponomarev, Soldagem Mig/Mag: Melhor entendimento, melhor desempenho, Artliber, 2008.
34. D.J. Kotecki, Braton N.R., and N.R. Loper, Preheat Effects on Gas Metal-Arc Welded Ductile Cast Iron, *Welding Journal*, 1969(48), 161 s-166 s.
35. F. Fernandes, B. Lopes, A. Cavaleiro, A. Ramalho, and A. Loureiro, Effect of Arc Current on Microstructure and Wear Characteristics of a Ni-Based Coating Deposited By Pta on Gray Cast Iron, *Surf. Coat. Technol.*, 2011, **205**(16), p 4094-4106

Publisher's Note Springer Nature remains neutral with regard to jurisdictional claims in published maps and institutional affiliations.